Bubble formation within filaments of melt-processed Bi2212 wires and its strongly negative effect on the critical current density

2011 Supercond. Sci. Technol. 24 075009

(http://iopscience.iop.org/0953-2048/24/7/075009)

Supercond. Sci. Technol. **24** (2011) 075009 (7pp) doi:10.1088/0953-2048/24/7/075009

Bubble formation within filaments of melt-processed Bi2212 wires and its strongly negative effect on the critical current density

F Kametani[1], T Shen[1,2], J Jiang[1], C Scheuerlein[3], A Malagoli[1], M Di Michiel[4], Y Huang[5], H Miao[5], J A Parrell[5], E E Hellstrom[1] and D C Larbalestier[1]

[1] Applied Superconductivity Center, National High Field Magnet Laboratory, Florida State University, Tallahassee, FL 32310, USA
[2] Fermi National Accelerator Laboratory, Batavia, IL 60510, USA
[3] European Organization for Nuclear Research (CERN), CH-1211 Geneva, Switzerland
[4] European Synchrotron Radiation Facility (ESRF), F-38043 Grenoble, France
[5] Oxford Superconducting Technology, Carteret, NJ 07008, USA

Received 28 March 2011
Published 16 May 2011
Online at stacks.iop.org/SUST/24/075009

Abstract
Most studies of $Bi_2Sr_2CaCu_2O_x$ (Bi2212) show that the critical current density J_c is limited by the connectivity of the filaments, but what determines the connectivity is still elusive. Here we report on the role played by filament porosity in limiting J_c. By a microstructural investigation of wires quenched from the melt state, we find that porosity in the unreacted wire agglomerates into bubbles that segment the Bi2212 melt within the filaments into discrete sections. These bubbles do not disappear during subsequent processing because they are only partially filled by Bi2212 grains as the Bi2212 forms on cooling. Correlating the microstructure of quenched wires to their final, fully processed J_c values shows an inverse relation between J_c and bubble density. Bubbles are variable between conductors and perhaps from sample to sample, but they occur frequently and almost completely fill the filament diameter, so they exert a strongly variable but always negative effect on J_c. Bubbles reduce the continuous Bi2212 path within each filament and force supercurrent to flow through Bi2212 grains that span the bubbles or through a thin Bi2212 layer at the interface between the bubble and the Ag matrix. Eliminating bubbles appears to be a promising new path to raise the J_c of Bi2212 round wires.

1. Introduction

The high-temperature superconductor (HTS) $Bi_2Sr_2CaCu_2O_x$ (Bi2212) is a promising material for high magnetic field applications. Short wire samples maintain a high critical current density J_c of $\sim 10^5$ A cm^{-2} at 4.2 K up to 45 T [1, 2], enabling superconducting magnets well beyond 23.5 T, the physical limit of Nb-based low-temperature superconductors, from which almost all present superconducting applications are made. Bi2212 is also the only HTS material capable of being made as a round wire that provides the preferred flexibility in magnet construction. Bi2212 round wire can exhibit high J_c without anisotropy in magnetic fields, has an irreversibility field H_{irr} greater than 100 T at 4.2 K [3] and can be fabricated by the powder-in-tube (PIT) method, first introduced for Bi2212 by Heine *et al* [4]. It is a suitable conductor for 20–50 T all-superconducting solenoids for >1 GHz nuclear magnetic resonance spectrometers [5], for muon cooling in a neutrino factory or a muon collider, and for >20 T dipoles and quadrupoles for high-energy hadron colliders [6].

Partial-melt processing is vital to develop high J_c [4]. The PIT conductor, whose filament powder starts as essentially single-phase Bi2212, is heated above the Bi2212 peritectic temperature in order to melt the Bi2212, which produces a liquid containing all the elements including Ag, as well as solid alkaline earth cuprate ($(Sr, Ca)_{14}Cu_{24}O_x$, AEC) and copper-

free ($Bi_9(Sr, Ca)_{16}O_x$, CF) phases. Slow cooling, in this case at 2.5 °C h^{-1}, solidifies this mixture by nucleation of Bi2212 grains below ∼872 °C. Manipulation of the overall Bi2212 composition and changing the cooling rate are some ways to raise J_c [7–10], but really much is still unknown about what controls J_c in wires. Recently we compared the separate contributions of superconducting connectivity and flux pinning to J_c by varying the cooling rate [11] through the Bi2212 phase nucleation in a through-process quench study. Reducing the cooling rate resulted in larger Bi2212 grains that better coupled between filaments. The physical connectivity of the filament pack was definitely enhanced by the larger Bi2212 grains. It appears that the superconducting connectivity was also enhanced because J_c increased significantly. Varying the cooling rate did not vary the flux pinning and thus had no effect on J_c, since the irreversibility field H_{irr}, evaluated by the extrapolated Kramer field H_K, was the same for all samples after they received a full, final oxygenation that put the 2212 grains into a reproducible, overdoped state [12].

However the specific connectivity-limiting mechanism(s) that control J_c are still elusive. Under the DOE-HEP-sponsored very high field superconducting magnet collaboration (VHFSMC), we have been investigating Bi2212 round wires with different wire architectures and fabrication methods [13]. Even though most of the wires used powder from the same source with the same chemical composition and were heat-treated similarly, J_c (4.2 K, 5 T) varied strongly, ranging between 1000 and 2880 A mm^{-2} for short samples 5–10 cm long. As is usually found, the 50–200 m lengths used for coils suffered J_c reductions of 20–50% compared to the 5–10 cm samples that were heat-treated at the same time. When we compare these wires that have widely varying J_c by magnetization, connectivity analysis using remnant magnetization and microstructural observations, there is almost no variation of flux pinning and microstructure among the conductors. We conclude, without having any explicit measure of the variables, that J_c varies because the connectivity varies greatly between the wires.

This unknown variation in connectivity drove us to search more carefully for its cause. We considered the presence of non-superconducting second phases like AEC and CF and also high-angle grain boundaries. These, however, are not the dominant, process-induced variables that explain the observed J_c variation. While performing this study, we started to quench samples just after they entered the melt phase and found that the distributed filament porosity had reorganized itself into well-defined bubbles. In this study, we focus on the role of these filament bubbles on J_c. Because polishing Ag–Bi2212 conductors is very hard to do without either filling the bubbles or pulling out parts of the filament, which mimics bubbles, we used two different techniques to observe the filaments. In the first we etched away the Ag matrix from the filaments and in the other we used synchrotron x-ray tomography to image the whole wire. Both observations agree: the residual powder porosity, typically 30–40%, agglomerates into bubbles on entering the melt state. We found that small pores agglomerate into large bubbles, which are as large as the filament diameter. These bubbles decrease the number of continuous Bi2212 grain-to-grain connections along the length of the filament after the full heat treatment. Finally we correlated the variation in J_c, which varied by about a factor of 4.5 from ∼600 to 2800 A mm^{-2} (4.2 K, 5 T), to the bubble density observed in polished cross sections of the fully processed wires, which varied from about 12 to 42 vol%. We found a strong inverse relationship between J_c and bubble density. We conclude that eliminating bubbles is an important pathway to increase J_c of Bi2212 round wires.

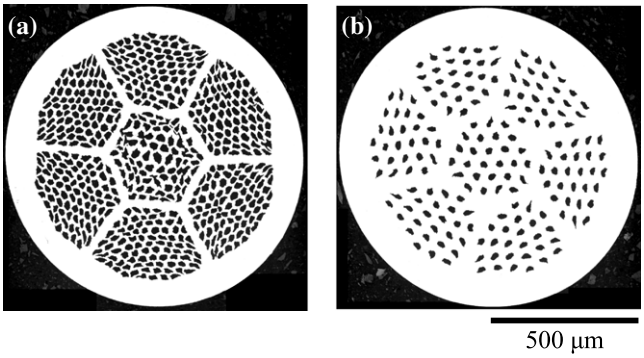

Figure 1. Transverse cross-sectional images of Ag-sheathed PIT multifilamentary Bi2212 round wires with (a) the 85 × 7 and (b) 27 × 7 architectures.

2. Experimental details

The Bi2212 multifilament round wires selected for most of this study are shown in figure 1. They were both fabricated by Oxford Superconducting Technology using the PIT technique. Figure 1(a) shows an 85 × 7 wire with filaments that are ∼20 μm in diameter, while figure 1(b) shows a specially designed 27 × 7 architecture in which 58 filaments in the 85-filament stack are replaced by solid Ag rods so as to maintain discrete Bi2212 filaments in the fully processed wire. The filaments are the same size in both conductors. We also studied a 37 × 18 wire.

4 cm long sections of wires were heat-treated using the heat treatment schedules shown in figure 2 in 1 bar flowing O_2. Samples were quenched from various points during the heat treatment, as indicated in figure 2, into room-temperature brine to freeze-in the high-temperature microstructure. For the 85 × 7 and 37 × 18 conductor, we examined the wires at various stages of partial-melt processing as shown in figure 2(a.) The sample designations are the following: unreacted (85-U/37-U), quenched at 872 °C (85-Q/37-Q) and fully processed (85-FP/37-FP). The designations for the 27 × 7 wires are similar: 27-Q887, 27-Q867, 27-Q862 and 27-FP (see figure 2(b)). Quenching was carried out using a vertical furnace. The wire ends were mechanically sealed to prevent BSCCO liquid from leaking out.

The 85 × 7 wire was dry-polished using a series of SiC papers with decreasing grit sizes. Final polishing was conducted in a 50 nm alumina suspension with the ethanol medium using an automatic vibratory polisher (Buehler Vibromet). As Ag is extremely soft after heating and the

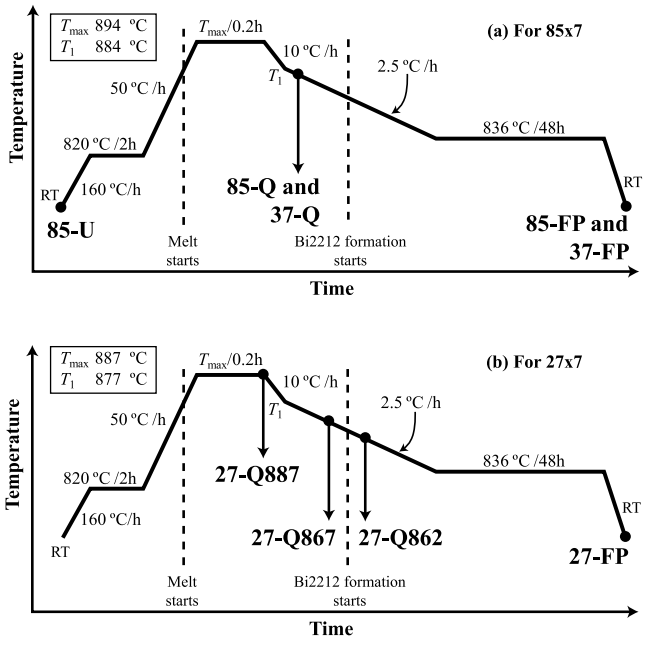

Figure 2. Schematic illustration of the heat treatment schedule for (a) the 85 × 7 and 37 × 18, and (b) the 27 × 7 wires. (a) 85-U and 85-FP/37-FP represent the unreacted and fully processed state of the 85 × 7 or 37 × 18 wire, respectively, whereas 85-Q/37-Q denotes the wires quenched from 872 °C. (b) The quench points for 27 × 7 are indicated as 27-Q887, 27-Q867 and 27-Q862.

Bi2212 filaments very porous and brittle, Ag is easily smeared into pores during the SiC polishing. We found that vibratory polishing is greatly superior to normal hand polishing because it helps to remove polishing debris and any smeared Ag in the pores.

The 27 × 7 wires were also polished in longitudinal cross section, finishing with a 6 μm diamond lapping film. They were then deeply etched in a 1:1:2 (volume) mixture of NH_4OH, H_2O_2 and methanol until undamaged filaments were exposed. Filament diameter in 27 × 7 was calculated from the average transverse cross-sectional filament area. Microstructures were examined in a scanning electron microscope (SEM) and the interior filament structure was revealed by using a focused-ion beam (FIB) in a Carl Zeiss 1540 EsB/XB using 30 kV Ga ions focused to a ∼200 nm diameter probe with 2 nA current.

Critical current I_c was measured on a series of fully processed wires using four-probe transport methods with a 1 μV cm^{-1} criterion at 4.2 K in a magnetic field of 5 T applied perpendicular to the wire axis. J_c was calculated using the oxide filament area determined from SEM cross sections of unreacted wires. All digital image manipulation was performed with the ImageJ program.

Synchrotron absorption microtomography was performed on 37 × 18 wire samples at the ID15A beam line of the European Synchrotron Radiation Facility (ESRF), using a monochromatic 70 keV x-ray beam. Due to the high flux of high-energy x-rays available at ID15A, tomograms of the highly absorbing Bi2212 samples can be achieved within less than one minute [14], which enables tomography during *in situ* heat treatments of the wires [15, 16]. Using the non-destructive tomography, polishing artifacts can be excluded, and in favorable cases a quantitative description of void volume can be obtained. The tomographic contrast corresponds to the volumetric x-ray absorption and thus is very appropriate for envisioning the very low density gas-filled bubbles in the Bi-containing phases and Ag that absorb x-rays much more strongly.

3. Results

3.1. 85 × 7 *wires*

Figure 3 illustrates the microstructure of the 85 × 7 wire at three key processing stages: 85-U, which is the as-fabricated wire (figure 3(a)); 85-Q, quenched after melting but before Bi2212 begins to form (figure 3(b)); and 85-FP, which is fully processed wire (figure 3(c)). 85-Q shows the frozen liquid phase, which contains ∼5 at.% Ag, and the AEC and CF phases. However, the most striking microstructural feature of 85-Q is the large density of pores (∼20 μm in diameter and ∼50–200 μm in length), which we call bubbles. On cooling, liquid, AEC and CF react with the liquid to form plate-like Bi2212 grains that occasionally penetrate the Ag matrix as outgrowths, but the reaction forming 2212 rarely goes to completion, leaving residual AEC and CF phases in the fully processed wire. In addition, in the fully processed Bi2212 wire (85-FP) about one-quarter of the filaments seen in cross section show remnants of bubbles (figure 3(c)). The longitudinal cross section of 85-FP (figure 3(c-longitudinal)) also shows residual porous regions similar to those seen in 85-Q872 (figure 3(b-longitudinal)).

3.2. 27 × 7 *wires*

Figure 4 shows the microstructure of the filaments from the 27 × 7 wires. As seen in the images, this specially designed, sparse-filament architecture allows us to extract individual filaments without the damage that would occur in the strongly inter-connected 85 × 7 wires. The filaments show in 3D the filament features that we could previously only see in 2D polished cross sections. Imaging the extracted filaments enables us to observe the filaments' porosity distribution and Bi2212 grain growth during the critical processing steps. As in the 85 × 7 wire, samples 27-Q887 and 27-Q867, which were quenched from the melt state, have filaments consisting of quenched liquid, the AEC and CF phase, and bubbles. Extracting individual filaments by etching away the Ag matrix, we could see the real structure of the filaments without any polishing artifacts. Figures 4(a) and (b) (27-Q887) show a continuous amorphous solid structure imprinted by grain boundary (GB) grooves from the Ag. These filaments contain large bubbles whose diameters are almost equal to the filament diameter. These bubbles segment the melt in each filament into discrete sections that are only a few filament diameters long. Based on the 42 bubbles in figure 4(a), which are distributed randomly along the filaments, the average center-to-center bubble separation is ∼144 μm. As seen in the larger magnification image of 27-Q887 in figure 4(b), it is clear that

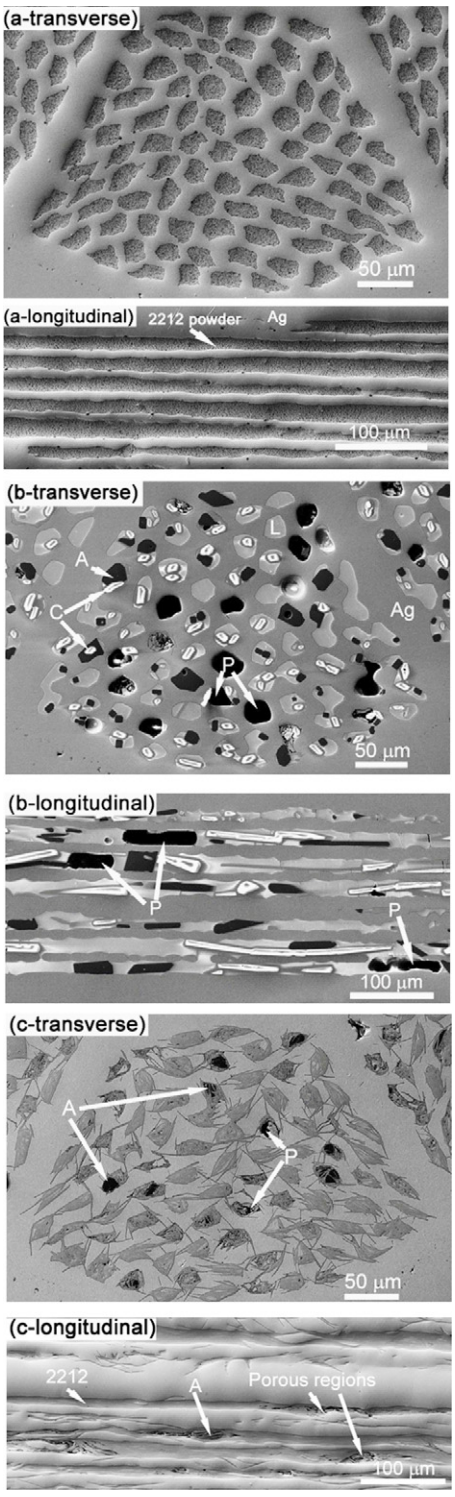

Figure 3. SEM images of the 85 × 7 wires at various stages of heat treatment: (a) 85-U—as-drawn, unreacted state, (b) 85-Q—quenched from the melt region at 872 °C, (c) 85-FP—fully processed state. Transverse and longitudinal cross sections are shown for each stage. L = liquid; A = AEC; C = CF and P = porosity.

the bubbles are completely hollow spaces. Some bubbles are quite spherical, ∼20 μm in diameter, while others seem to be agglomerates of several bubbles whose lengths (∼50–100 μm) are several times the filament diameter.

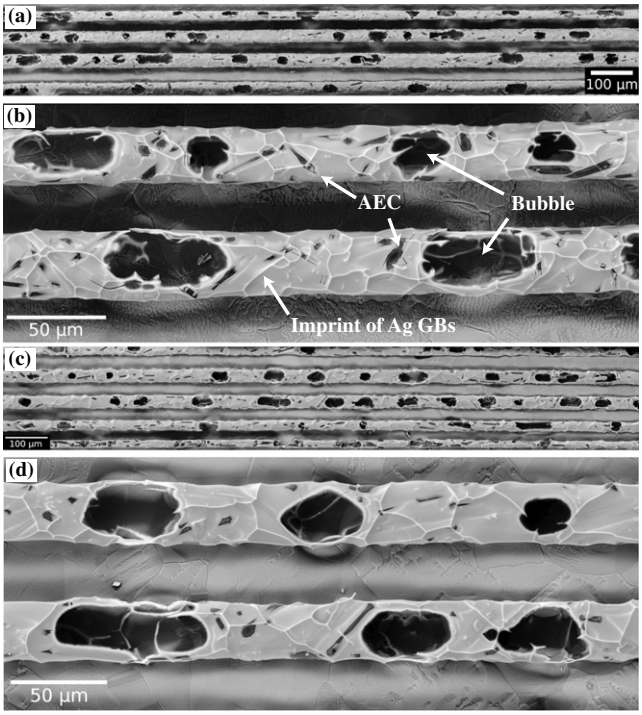

Figure 4. SEM images of the filaments in the 27 × 7 wires quenched from (a) and (b) the melt state at 887 °C (27-Q887) and (c) and (d) from 867 °C (27-Q867), just above the Bi2212 re-formation onset temperature. Large bubbles almost completely fill the filament diameter at many places with a quite non-uniform distribution.

Figures 4(c) and (d) show the microstructure of 27-Q867, which was quenched just before re-formation of the Bi2212. The bubbles are still present and there is no sign that they are being redistributed, eliminated or shrinking, as judged by an almost unchanged bubble density: approximately 70 bubbles cm^{-1}, compared to 69 bubbles cm^{-1} in 27-Q877 (figure 4(a)).

The microstructure drastically changes when Bi2212 starts to re-form on cooling, as seen in sample 27-Q862 (figure 5), where the microstructure is now a mixture of frozen liquid and Bi2212. Since 27-Q862 is quenched just under the temperature where Bi2212 starts to re-form, lots of liquid is still present judging from the clear Ag grain boundary imprints on the surface of the filament. In addition there are straight line contrasts in figure 5 that are from the large, plate-like Bi2212 grains growing under the liquid. This indicates that the Bi2212 grains do not necessarily form only at the Ag interface. An important microstructural change is that the filaments in 27-Q862 are continuous and no bubble is visible from the filament exterior.

However, the bubbles have not disappeared in 27-Q862. Figure 6 shows SEM images in a different location on the same filament of figure 5 (27-Q862). No bubbles are seen from the filament exterior of figure 6(a). However the internal microstructure exposed by FIB reveals that remnants of the bubbles still exist even after the 2212 begins to form (figure 6(b)). For figure 6, the region surrounded by the white dotted line in figure 6(a) was FIBed and then tilted in such a way that the FIBed cross section can be seen. It clearly shows

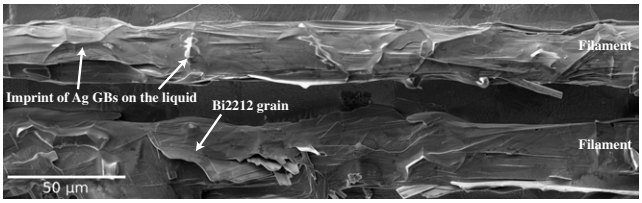

Figure 5. SEM images of the filaments in the 27 × 7 wires quenched from 862 °C (27-Q862), just below the Bi2212 re-formation temperature, showing a mixture of Bi2212 and residual liquid. Bi2212 grains have formed inside the filament and appear to have left a liquid 'skin' at the interface with the Ag in many places.

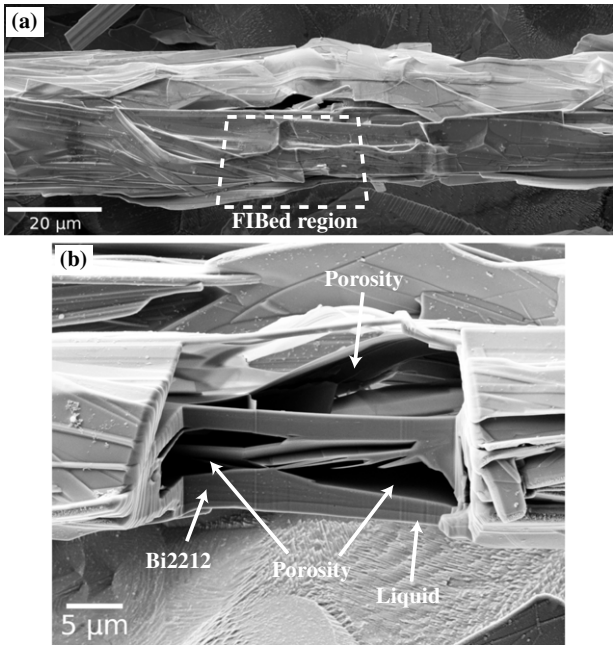

Figure 6. SEM images of a different location on the same filament of figure 5 (27-Q862). (a) The filament exterior showing no bubbles. The FIBed region is indicated by the white dotted line. (b) FIBed cross section revealing the porous microstructure inside the filament.

a porous filament microstructure in which long, but thin, plate-like Bi2212 grains have grown across the bubbles, dividing the bubbles and partially filling them. The Bi2212 grains that span the bubbles partially reconnect the melt regions separated by the bubble. However this reconnection is imperfect. Figure 6 shows that about half of the cross section is still porous and the current path is limited to an outer shell of Bi2212 near the Ag interface and several large Bi2212 grains that are 1–2 μm thick in the center. Considering that there is no liquid inside the bubbles (see figures 4(a)–(d)), which is necessary to form Bi2212, it is unlikely that Bi2212 can completely fill the bubbles in the later stages of the heat treatment.

3.3. 37 × 18 *wires*

We used x-ray synchrotron microtomography to image the porosity in quenched and fully processed 37 × 18 wires. Figure 7 shows transverse and longitudinal cross sections of 37-Q, quenched before 2212 began to form on cooling, and 37-FP. The darkest and lightest areas in these cross sections

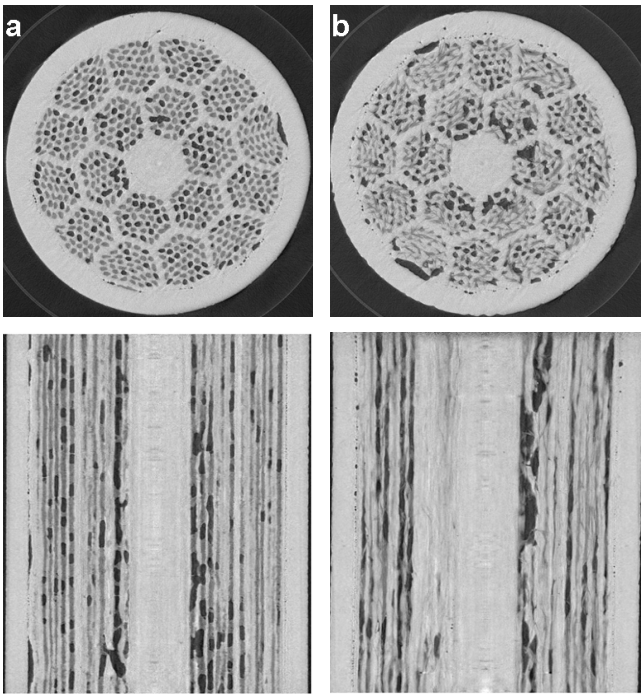

Figure 7. Tomographic transverse (top) and longitudinal (bottom) cross sections of a 37 × 18 wire that was (a) quenched from 887 °C just before 2212 began to re-form (37-Q) and (b) in the fully processed state (37-FP). The darker gray regions are bubbles, the mid-gray regions are Bi2212 or other phases that can be formed from Bi, Sr, Ca, Cu and O, and the brightest regions represent Ag. Delamination of the outer Ag sheath from the inner Ag bundle can be seen in both tomograms. The wires are 0.8 mm in diameter.

represent the bubbles (no x-ray absorption) and the most strongly absorbing Ag matrix, respectively. The mid-gray areas are the Bi2212, Bi-2201, AEC and CF, which all absorb x-rays less than Ag.

The tomograms clearly show that the filaments contain a large fraction of bubbles. The shape and distribution of the bubbles in 37-Q (figure 7(a)) are very similar to those seen in 85-Q (figure 3(b)), thus validating our improved polishing techniques. But figure 7 exhibits more clearly the non-uniform distribution of bubbles along individual filaments and shows more bubbles in the inner filament bundles. Comparing the longitudinal tomograms of 37-Q and 37-FP in figure 7 confirms the observation of figure 6 that 2212 grain growth does not eliminate the bubbles. It is also interesting that the tomogram of 37-FP shows agglomerated porosity, including bubbles that are larger than a single filament after Bi2212 re-formation. Clearly a large volume of bubbles remains in the fully processed wire (figure 7(b)), which significantly limit J_c.

4. Discussion

The microstructures shown here of the 85 × 7, 37 × 18 and 27 × 7 wires provide us a quite new view of what happens in the melt. Although it has been known for a long time that the filaments in powder-in-tube-processed wires are not fully dense, it has generally been thought that the residual 30–40 vol% porosity [17, 18] filled in during the heat

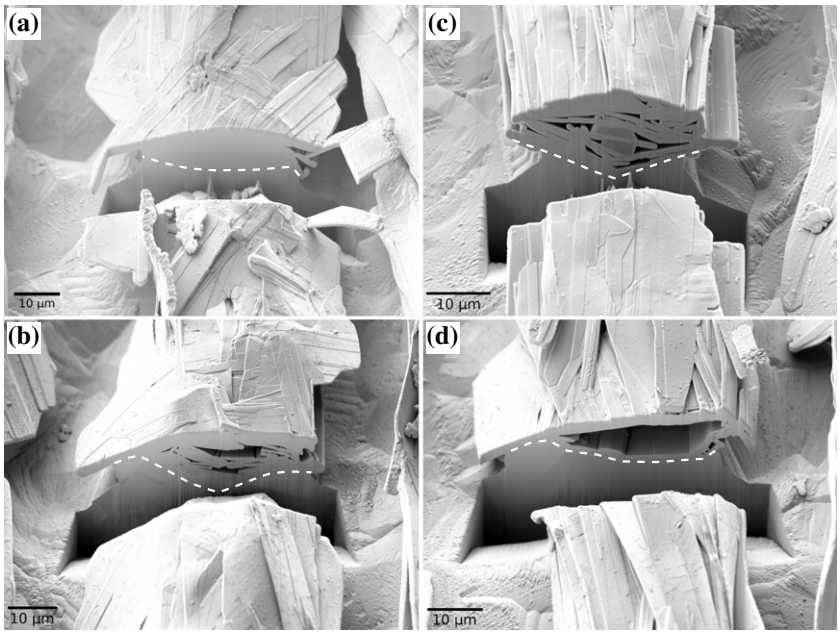

Figure 8. FIBed transverse cross-sectional images of different locations on the same filament taken from the 27 × 7 wire 27-FP, showing (a) a completely dense structure inside the filament, (b) and (c) small pores in the center of the filament which reduce an effective cross section for current flow and (d) the hollow core and shell of Bi2212 in contact with Ag which may be assumed to carry supercurrent well. Dotted lines represent the approximate interface between filaments and Ag.

treatment. What the present observations make clear is that the residual porosity in Bi2212 filaments agglomerates on entering the melt state, making bubbles that are frequent and largely block the whole filament (figures 3 and 4), are not removed during the heat treatment and clearly have the ability to strongly suppress the current paths in each filament. The number, volume fraction and distribution of bubbles are almost unchanged until the Bi2212 grains start to re-form when it is seen that many Bi2212 grains can span the bubbles, allowing all wires to carry supercurrent. The fully processed 27 × 7 wires are interesting because there are no filament-to-filament bridges that would potentially allow supercurrent transfer around such bubbles, but even so this wire has an I_c of ∼120 A at 4.2 K and self-field because, as shown in figure 6, the bubbles are partially filled by Bi2212, allowing at least a partial connectivity across the bubbles.

If the source of bubbles is most plausibly some combination of gas filling the residual 25–30% porosity of the filaments, carbonaceous impurities or even the O_2 evolved on 2212 melting, the key step that makes Bi2212 different from, for example, MgB_2 is that there is a large melt phase. This liquefaction of the filaments allows the subdivided gas pores to agglomerate into bubbles which reduce the surface energy of gas in the liquid. In 85 × 7 and 37 × 18 wires where the filaments are very closely packed, some dissolution of the inter-filament Ag also occurs, allowing filaments to bond and so bubbles in adjacent filaments agglomerate into bubbles with diameters greater than a single filament [11]. Recently we also have found another negative effect of the bubbles. During the heat treatment, the internal pressure of the confined gas pushes the liquid toward both ends of wires, decreasing the local mass density of Bi2212 in the middle part of the wire and significantly reducing I_c [19]. This seems to be the fundamental cause of the broadly observed lower 20–30% I_c measured in 1 m, as opposed to 5–10 cm, long samples.

The non-destructive synchrotron x-ray tomograms of figure 7 confirm that the macroscopic inhomogeneity deduced both from polished cross sections and isolated filaments is very similar. At the individual filament level, the non-uniform distribution of bubbles also results in a local inhomogeneity of the final microstructure that suppresses the connectivity of the wires after the full heat treatment. Figure 8 shows this using FIBed transverse cross-sectional images at four different locations in the same filament from a 27-FP wire. Figure 8(a) shows an almost 100% dense microstructure, meaning that the I_c of this section is dependent principally on the grain boundary properties, which can be significantly ameliorated by overdoping [12]. However, the three other images reveal porous structures inside the filament, the worst case being shown in figure 8(d) where the filament is a hollow shell, greatly suppressing connectivity by reduction of physical grain-to-grain connections. When the Bi2212 grains grow across the bubbles, material is transferred out of the melt and into the bubble regions. The Bi2212 grains divide the bubbles into smaller regions and the mass transfer into the bubbles is accompanied by the formation of porosity in initially dense melt regions. Although the Bi2212 grains appear in the center of the cross sections of figures 8(b) and (c), their connections to outer Bi2212 layers are so thin that we suppose that the local I_c is very small. Speculations on the importance of the Ag–Bi2212 interface layer have been made before [20]: it does appear from the present observations that there is a continuous thin layer at this interface and presumably this is important for I_c. But clearly the route to higher J_c requires a fuller utilization

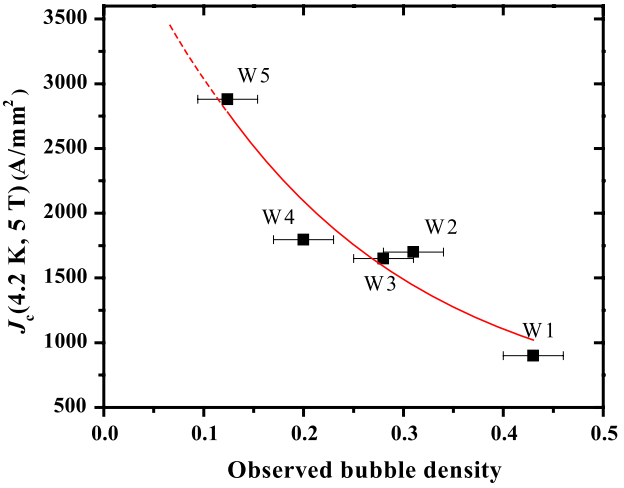

Figure 9. J_c (4.2 K, 5 T) for various wires of recent vintage plotted as a function of their bubble density, approximated by the volume fraction of bubbles visible in wires quenched from the melt region at T_{max}. Samples were heated to 887 °C and held for 12 min before being quenched. W1 is a single-restack wire 0.8 mm in diameter with 1050 filaments. W2, W3 and W5 are 37 × 18 wires of 0.8 mm diameter, while W4 is a 85 × 7 wire of 1.06 mm diameter. All wires were made from the same precursor powder.

(This figure is in colour only in the electronic version)

of the bulk connectivity of the whole filament and this is highly variable. Since the I_c of the wire is determined by bottlenecks at the filament level, it is reasonable to suppose that the most porous regions like those in figure 8(d) determine the actual I_c of the filaments.

As a first attempt to estimate the benefits of strongly reducing the bubble density, we accumulated data on bubble density and J_c from several recent industrial wires that we have been studying, which is shown in figure 9. The bubble density was evaluated from the total area fraction of bubbles in samples quenched from the melt, which is derived from digital image analysis of the transverse cross-sectional images. We evaluated quenched samples since figure 7 shows that for some wires, the bubble inhomogeneity can be greater in the fully processed wire than in a wire quenched from the melt state. We do not yet understand the correlation between J_c and bubble density, but it is clear that J_c sharply increases with decreasing bubble density, indeed showing the bubble density is an important processing variable for J_c. Recent attempts at reducing the bubble density have been quite successful—we doubled I_c in the 27 × 7 wire studied here when we applied specific processing aimed at reducing the bubble density.

5. Conclusion

In summary, we identified agglomerated porosity (bubbles) as a major current-blocker in Ag-sheathed, PIT multifilamentary Bi2212 round wire. By studying how microstructure develops through processing, we revealed that bubbles of agglomerated porosity appear in the wire only upon melting of the Bi2212 powder. The consequences are major: the Bi2212 filaments become subdivided into discrete segments, greatly reducing their long-range connectivity, though Bi2212 grains can partially fill the bubbles on cooling back into the solid state. We conclude that densifying Bi2212 wires is a key approach to improving Bi2212 J_c, where in fact the critical current density is controlled more by poor connectivity than by flux pinning.

Acknowledgments

We are very grateful to discussions within the Very High Field Superconducting Magnet Collaboration. The work was supported by the VHFSMC, an ARRA grant of the US Department of Energy and by the National High Magnetic Field Laboratory which is supported by the National Science Foundation under NSF/DMR-0084173 and by the State of Florida. We also acknowledge the ESRF for beam time on the ID15A beamline.

References

[1] Miao H, Marken K R, Meinesz M, Czabaj B and Hong S 2005 *IEEE Trans. Appl. Supercond.* **15** 2554–7
[2] Marken K R, Miao H, Meinesz M, Czabaj B and Hong S 2003 *IEEE Trans. Appl. Supercond.* **13** 3335–8
[3] Chen B, Halperin W P, Guptasarma P, Hinks D G, Mitrovic V F, Reyes A P and Kuhns P L 2007 *Nature Phys.* **3** 239–42
[4] Heine K, Tenbrink J and Thoner M 1989 *Appl. Phys. Lett.* **55** 2441–3
[5] Markiewicz W D, Miller J R, Schwartz J, Trociewitz U P and Weijers H W 2006 *IEEE Trans. Appl. Supercond.* **16** 1523–6
[6] Godeke A *et al* 2008 *IEEE Trans. Appl. Supercond.* **18** 516–9
[7] Kumakura H, Kitaguchi H, Togano K and Sugiyama N 1996 *J. Appl. Phys.* **80** 5162
[8] Zhang W and Hellstrom E E 1995 *Supercond. Sci. Technol.* **8** 430–8
[9] Motowidlo L R, Galinski G, Ozeryansky G, Zhang W, Hellstrom E E, Sumption M and Collings T 1995 *IEEE Trans. Appl. Supercond.* **5** 1162–6
[10] Holesinger T G, Kennison J A, Marken K R, Miao H, Meinesz M and Campbell S 2005 *IEEE Trans. Appl. Supercond.* **15** 2562–5
[11] Shen T, Jiang J, Kametani F, Trociewitz U P, Larbalestier D C, Schwartz J and Hellstrom E E 2010 *Supercond. Sci. Technol.* **23** 025009
[12] Shen T, Jiang J, Yamamoto A, Trociewitz U P, Schwartz J, Hellstrom E E and Larbalestier D C 2009 *Appl. Phys. Lett.* **95** 152516
[13] Jiang J, Myers D, Shen T, Kametani F, Trociewitz U P, Hellstrom E E and Larbalestier D C 2010 'Comparative studies of nine new Bi-2212 round wires' 2MX-03 *Applied Superconductivity Conf. (Washington, DC MD)*
[14] Di Michiel M, Merino J M, Fernandez-Carreiras D, Buslaps T, Honkimäki V, Falus P, Martins T and Svensson O 2005 *Rev. Sci. Instrum.* **76** 043702
[15] Scheuerlein C, Di Michiel M and Buta F 2009 *IEEE Trans. Appl. Supercond.* **19** 2653
[16] Scheuerlein C, Di Michiel M and Haibel A 2007 *Appl. Phys. Lett.* **90** 132510
[17] Malagoli A, Kametani F, Jiang J, Trociewitz U P, Hellstrom E E and Larbalestier D C 2011 *Supercond. Sci. Technol.* accepted
[18] Tenbrink J, Wilhelm M, Heine K and Krauth H 1991 *IEEE Trans. Magn.* **27** 1239
[19] Karuna M, Parrell J A and Larbalestier D C 1995 *IEEE Trans. Supercond.* **5** 1279
[20] Holesinger T 2006 Characterization of Oxford Bi2212 conductors *Low Temperature Superconductor Workshop (Tallahassee, FL)*